Theoretical Study of Mechanisms, Thermodynamics, and Kinetics of the Decomposition of Gas-Phase α-HMX (Octahydro-1,3,5,7-tetranitro-1,3,5,7-tetrazocine)

Shaowen Zhang, Hung N. Nguyen, and Thanh N. Truong*

Henry Eyring Center for Theoretical Chemistry, Department of Chemistry, University of Utah, 315 S 1400 E, Room 2020, Salt Lake City, Utah 84112

Received: January 10, 2003

We present a theoretical study of the decomposition mechanism of gas-phase α-HMX. Four distinct channels were studied using the B3LYP/cc-pVDZ level of theory. These are as follows: (i) HMX first loses an NO_2 to form HMR which further breaks a C−N bond to form a chain structure and then later loses three methylenenitramines (MN, H_2CNNO_2) successively; (ii) the chain structure forms a 10-member ring via a rung closure step before undergoing further decomposition; (iii) HMX first eliminates an HONO, then loses two MN, and eliminates an HONO successively; (iv) HMX eliminates two HONO successively, then loses an MN, and finally eliminates an HONO. The rate constants of each elementary reaction have been calculated using the transition-state theory. The thermodynamics properties were also calculated for the stable species by employing a standard statistical thermodynamics method. Channel i was found to be the preferred decomposition pathway on the basis of the analysis of rate constants of the elementary reactions.

1. Introduction

The cyclic nitramines octahydro-1,3,5,7-tetranitro- 1,3,5,7-tetrazocine (HMX) and hexhydro-1,3,5-trinitro-1,3,5-triazine (RDX) have been widely used in various propellants and explosives due to their physical properties. Understanding the fundamental chemical mechanism and kinetics of the combustion or detonation processes of these materials is important for further improvement in the use of these materials. However, due to the energetic nature of these materials, the decompositions are so fast and complex[1,2] that it is difficult to experimentally explore the chemical details of these processes. In recent years, with the advance in computer technology and computational quantum chemistry methods, especially the development of the density functional theory, it is possible to predict the energetic nature of these reactions with high accuracy for larger molecules such as HMX.

In the past several years, theoretical studies of nitramines mainly concentrated on smaller molecules and RDX.[3−9] Few theoretical results have been reported concerning the decomposition mechanism of HMX.[2,10−14] Melius studied the gas-phase decomposition mechanism using the empirically corrected ab initio quantum chemistry method BAC-MP4.[12] He concluded that a $N-NO_2$ bond fission reaction occurs at high temperature and HONO elimination occurs at low temperature. Lewis and co-workers[11] calculated the initial steps of four possible decomposition pathways of HMX using BLYP and B3LYP DFT methods with the 6-311G(d,p) basis set. The four pathways are $N-NO_2$ bond fission, HONO elimination, C−N bond scission of the ring, and the concerted ring fission. According to their results, the $N-NO_2$ bond fission path is the dominant initial step of the decomposition of gas-phase HMX. Chakraborty and co-workers[10] calculated the unimolecular decomposition mechanism of β-HMX using the B3LYP/6-31G(d) method. They identified three distinct channels: (1) a $N-NO_2$ bond fission reaction to form NO_2 and HMR, which subsequently decomposes to various products through several subsequent pathways; (2) successive HONO elimination to give four HONO plus a stable intermediate; and (3) oxygen migration from one of the NO_2 groups of HMX to a neighboring carbon atom followed by decomposition steps. Among these three pathways, the $N-NO_2$ bond fission path has the lowest barrier in the initial step. We have in fact performed an accurate direct dynamics study on the kinetics of the $N-NO_2$ bond fission reaction using the microcanonical variational transition-state theory with the B3LYP/cc-pVDZ potential energy surface. The predicted thermal rate constants are in agreement with experimental results.[13] We also studied the branching ratio and pressure-dependent rate constants of the $N-NO_2$ bond fission path and HONO elimination path with the master equation method and found that the $N-NO_2$ bond fission path dominates the reaction at high-pressure limits.[14]

Experimental studies of HMX were mainly concentrated on the condensed phase. Various species (for example $m/e = 250$, 249, 222, 205, 176, 175, 148, 128, 120, 102, 97, 81, 75, 74, 70, 56, 54, 47, 46, 45, 43, 42, 32, 30, 28) have been identified in different decomposition experiments of HMX using mass spectra techniques.[15−22] These results indicate that the decomposition of HMX is very complicated and may undergo different mechanisms in different conditions. Brill[23] has suggested two global pathways in the thermal decomposition of HMX in the condensed phase:

$$\mathrm{HMX} \rightarrow 4(\mathrm{HOHO} + \mathrm{HCN})$$

$$\mathrm{HMX} \rightarrow 4(\mathrm{H_2CO} + \mathrm{NNO})$$

Tang and co-workers also concluded[22] that a multistep mechanism might be more realistic in explaining the experimental data in their laser-assisted self-burning experiment of the condensed-phase HMX. On the basis of his pyrolysis results of HMX determined by simultaneous thermogravimetric modulated beam mass spectrometry technique, Behrens proposed a mechanism[24] where HMX first decomposes via the N−N bond

10.1021/jp030032j CCC: $25.00
Published on Web 04/01/2003

fission, followed by ring fragmentation, and decomposes to NNO and H_2CO:

$$HMX \rightarrow NO_2 + H_2CN + 3H_2CNNO_2$$

$$H_2CNNO_2 \rightarrow NNO + H_2CO$$

This mechanism is similar to that proposed by Melius.[12]

Clearly, little is known about the early stage of the decomposition of HMX beyond the first step. In this study, we present a systematic DFT study on several low-lying energy pathways of the decomposition of gas-phase HMX. Furthermore, the rate constants of the elementary reactions involved in the pathways, as well as the thermodynamic parameters of stable species, were calculated. Thus the new mechanism can be readily used in simulations of macroscopic observables.

2. Methodology

2.1. Thermal Rate Constants. Within the transition-state theory (TST) framework,[25] thermal rate constants of a reaction can be expressed as

$$k(T) = \kappa(T)\sigma\frac{k_B T}{h}\frac{Q^{\ddagger}(T)}{\Phi^R(T)}e^{\{-\Delta V^{\ddagger}/kBT\}} \quad (1)$$

where κ is the transmission coefficient accounting for the quantum mechanical tunneling effects; σ is the reaction symmetry number; $Q^{\ddagger}$ and Φ^R are the total partition functions (per unit volume) of the transition state and reactants, respectively; $\Delta V^{\ddagger}$ is the classical barrier height; T is the temperature; and k_B and h are the Boltzmann and Planck constants, respectively. Several steps involve hydrogen-transfer processes. For such steps, tunneling is expected to be noticeable. The one-dimensional Eckart tunneling method was employed to calculate the transmission coefficient κ. All rate constant calculations were performed using our online Virtual Kinetic Laboratory (VKLab).[26]

2.2. Thermodynamic Properties. Statistical thermodynamics methods[27] were employed to calculate the standard entropies ($S°$) and pressure heat capacities (C_p). To obtain the standard heat of formation at 298 K with better accuracy, we first write a reaction to produce the considered compound from simple species whose standard heats of formation were well-known. Then we calculate the reaction energy utilizing quantum chemistry methods with the thermal correction at 298 K using standard statistical methods. The heat of formation at 298 K of the considered molecule is then calculated from these data. The calculated standard entropies, constant-pressure heat capacities, and standard enthalpy are given in the CHEMKIN format using the following polynomial expressions:[28]

$$C_p/R = a_1 + a_2T + a_3T^2 + a_4T^3 + a_5T^4 \quad (2)$$

$$\frac{H°}{RT} = a_1 + \frac{a_2}{2}T + \frac{a_3}{3}T^2 + \frac{a_4}{4}T^3 + \frac{a_5}{5}T^4 + \frac{a_6}{T} \quad (3)$$

$$\frac{S°}{R} = a_1 \ln T + a_2T + \frac{a_3}{2}T^2 + \frac{a_4}{3}T^3 + \frac{a_5}{4}T^4 + a_7 \quad (4)$$

All thermodynamics calculations were done using VKLab.[26]

2.3. Electronic Structure Calculations. Earlier studies have shown that the hybrid density function theory can provide reasonably accurate prediction of the information along the reaction path. In particular, Johnson et al.[5] recently reported that Becke's three parameter functional with Lee, Yang, and Parr's correlation functional (B3LYP))[29] performs well in predicting stationary-point geometries in comparison with those from the QCISD method in a study of the decomposition mechanism of dimethylnitramine (DMNA). In this study, all the calculations were carried out using the B3LYP method in conjunction with Dunning's correlation-consistent double-ζ basis set (cc-pVDZ)[30] that was also demonstrated to be an effective basis set in Johnson et al.'s study. Unrestricted method (UB3LYP) was used for calculations involving radicals. The singlet open-shell B3LYP method with mixed frontier molecular orbitals was adopted to calculate the species that have biradical characters. All the stationary points have been verified from normal-mode analyses. In particular, each transition state has only one imaginary frequency whose vibrational mode points to the corresponding reactant and product and each stable species has all possitive frequencies. The calculated frequencies were further employed to calculate thermodynamics properties and rate constants. All calculations were performed using the GAUSSIAN98 program.[31]

3. Results and Discussion

3.1. Reaction Mechanism. HMX has four crystalline polymorphs, α, β, γ, and δ, among which α, γ, and δ polymorphs have similar boatlike conformations that are different from the chairlike conformation of the β polymorph. The β polymorph is stable at room temperature,[32] and α and δ polymorphs are stable at higher temperature ranges.[33,34] According to previous theoretical study,[13] the three boatlike conformations (α, γ, and δ) merge to one conformation that has C_{2v} symmetry (denoted as α-HMX hereafter) in the gas phase. Chakraborty et al. have studied the gas-phase thermal decomposition mechanism of β-HMX. In this paper, we report the gas-phase thermal decomposition mechanism of α-HMX.

So far, three distinct initial decomposition pathways have been identified for gas-phase HMX.[10,11] The first pathway is the concerted ring cleavage that leads to four methylenenitramine (MN). MN further decomposes into smaller stable species. The second pathway is initiated by the breaking of an $N-NO_2$ bond. The third pathway is initiated by an HONO elimination reaction. The concerted ring cleavage channel has been found to have a large barrier in a previous study,[11] and thus it will not be reiterated here. However, the last two channels, which may dominate the decomposition of HMX, are rather complicated due to different subsequent branching. To explore such branching at each stable intermediate, a bond order analysis was done to identify several of the weakest bonds. Further decomposition pathways from these weak bonds are then followed. Here several new low-lying energy pathways are presented, yielding stable intermediates that have been identified by experiments.[11,24,35]

3.1.1. $N-NO_2$ Fission Pathway. The $N-NO_2$ bond is believed to be the weakest bond in HMX despite scattered bond dissociation energies reported by both theoretical and experimental studies.[2,3,10−14] Figure 1 shows a schematic illustration of the decomposition mechanism of the $N-NO_2$ fission path. The corresponding energy profiles of this path are depicted in Figure 2. The relative electronic energies are provided together with the zero-point-energy (ZPE) corrected relative energies (in parentheses) in Figure 2. Notice that in the calculation of the relative energies, the zero of energy is at the reactant, HMX.

Following the same naming convention in Figure 1, in this pathway HMX first evolves to HMR after losing a NO_2 molecule via an endothermic process without a barrier. HMR next breaks the second-nearest-neighbor C−N bond and be-

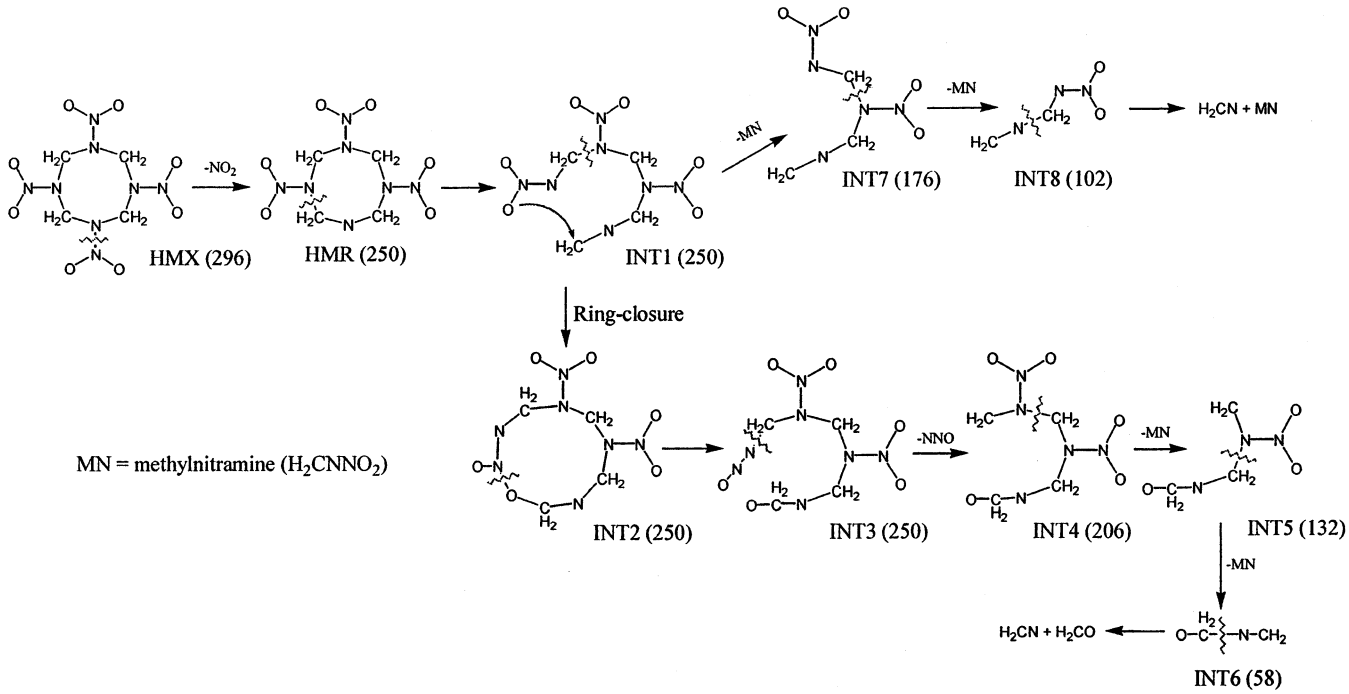

Figure 1. Schematic diagram of the $N-NO_2$ fission pathway. The molecular masses of the species are provided in parentheses.

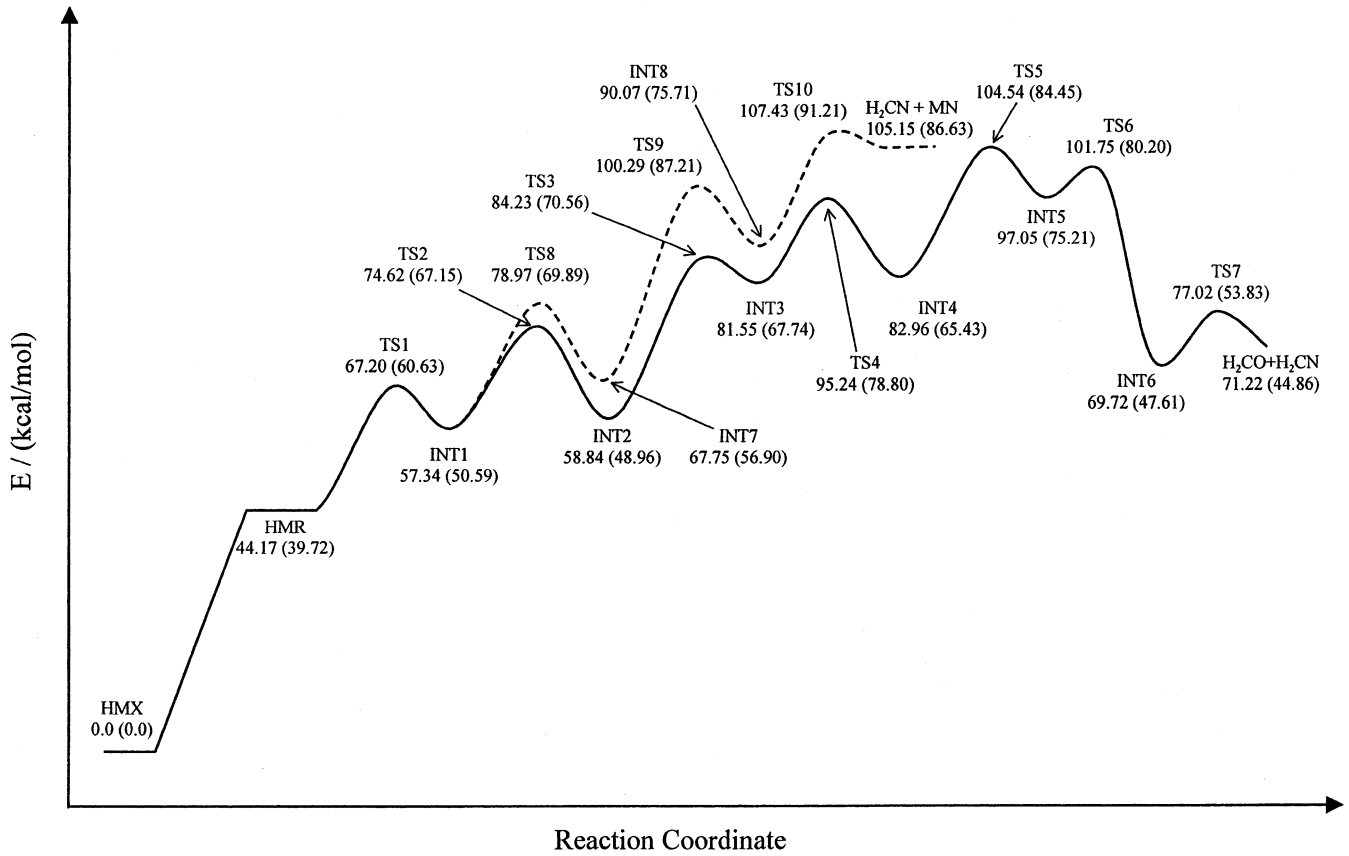

Figure 2. Relative energies of the $N-NO_2$ fission pathway. The data in parentheses are zero-point-energy corrected relative energies. See Figure 1 for notations of species.

comes a chain-structure molecule (INT1) after passing a transition state (TS1) at the second step. These two steps are in agreement with previous studies. Melius estimated the bond dissociation energy of $N-NO_2$ to be about 46 kcal/mol in a BAC-MP4 study.[12] Earlier DFT studies predicted this energy to be 40.5,[11] 39.8,[10] and 39.7[13,14] kcal/mol at B3LYP/6-311g-(d,p), B3LYP/6-31g(d), and B3LYP/cc-pVDZ levels of theory, respectively. All relative energies include ZPE corrections. This is held throughout the discussion unless specified. The predicted barrier height of the second step is somewhat scattered. Melius's BAC-MP4 calculation[12] and Chakraborty's B3LYP/6-31g(d) calculation[10] predicted the barrier height to be 17.9 and 28.0

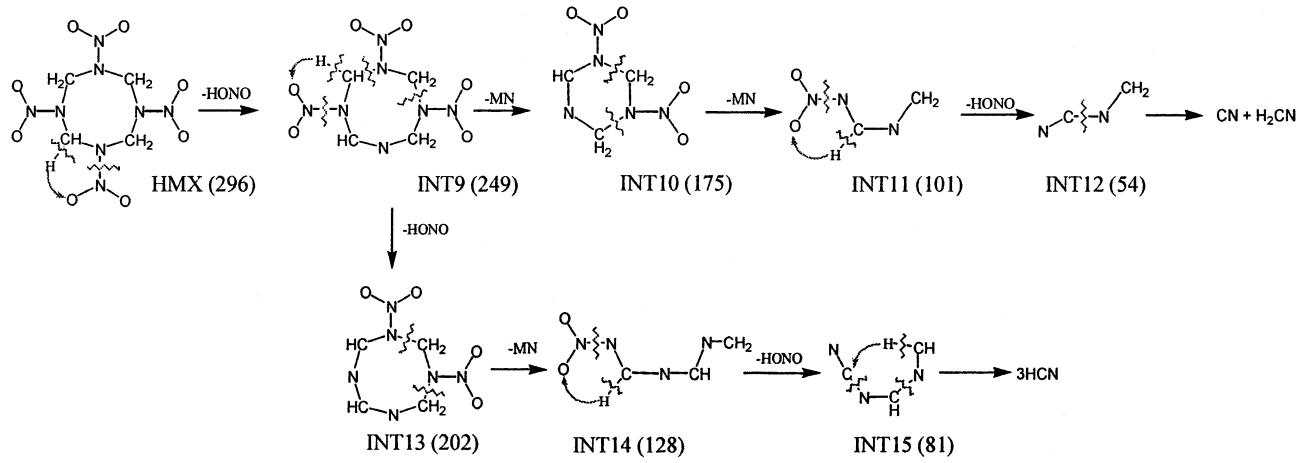

Figure 3. Schematic diagram of HONO elimination pathway. The molecular masses of the species are provided in parentheses.

kcal/mol, respectively. Our result of 20.9 kcal/mol is in better agreement with BAC-MP4's value. This comparison also validates the accuracy of the level of theory used in this study.

The chain-structure INT1 may be a key species in the decomposition of HMX due to its flexibility and may thus undergo different further decomposition pathways. In this study, we examined two low-lying energy pathways.

In the first pathway, INT1 proceeds with a ring closure between the oxygen atom of the neighboring NO_2 group in INT1, connecting with the nearby carbon atom obtained from the breaking of the C−N bond in the proceeding step to form a 10-member ring (INT2) by surmounting the transition state (TS2) with a relatively low barrier height of 16.6 kcal/mol. The O−N bond in INT2 then breaks, and the ring reopens to form INT3 through the transition state TS3. The barrier of this step is 21.6 kcal/mol. INT3 loses an NNO molecule, which is an important final product in HMX decomposition, to form INT4 through the transition state TS4 with the barrier height of 11.1 kcal/mol. INT4 then loses two MN successively to form INT5 and INT6 by passing TS5 and TS6 transition states. The barrier heights of these two steps are 19.0 and 5.0 kcal/mol, respectively. Finally, INT6 decomposes to H_2CO and H_2CN via the transition state TS7 with a small barrier of 6.2 kcal/mol. Notice that from a previous study, with the assistance of a water molecule, MN can easily decompose to H_2CO and NNO with a barrier lower than 10 kcal/mol.[12] For each mole of HMX at this stage of the decomposition the final products are 1 mol of NO_2 and of H_2CN and 3 mol of H_2CO and of NNO,

$$\mathrm{HMX} \rightarrow \mathrm{NO_2} + \mathrm{H_2CN} + 3\mathrm{H_2CO} + 3\mathrm{NNO}$$

The above reaction is exothermic with the total ZPE corrected reaction energy of about −24.2 kcal/mol. Once these products are formed, the energy release sustains further decomposition of HMX. Moreover, all barrier heights along this path are lower than that of the initial step. Thus, the N−NO_2 bond fission is the rate-limiting step.

The second pathway is similar to that proposed by Melius[12] and Behrens.[24] INT1 successively loses three MN via TS8, INT7, TS9, INT8, and TS10, respectively. The final products of this pathway are the same as in the first pathway. The barrier heights of TS8, TS9, and TS10 are 19.3, 30.3, and 15.5 kcal/mol, respectively. These barrier heights are also lower than that of the initial step.

Both pathways in the N−NO_2 fission path are quite promising due to the low barrier heights of the subsequent steps. In addition, the distribution of products of these two pathways is in agreement with experimental observations that 3 mol of NNO are measured for each mole of decomposed HMX.[24]

3.1.2. HONO Elimination Path. The HONO elimination pathway is initiated by an HONO elimination reaction. Although Chakraborty and co-workers[10] have studied the successive elimination reaction of four HONO in this pathway, detailed knowledge of this pathway is still limited. Figures 3 and 4 depict the schematic diagrams of the decomposition mechanism and corresponding energy profiles of the HONO elimination path, respectively.

At the initial step, an oxygen atom of an NO_2 group of HMX abstracts a hydrogen atom of a neighbor CH_2 group to produce an intermediate INT9 via the transition state TS11. The barrier height of this step is 42.4 kcal/mol. This barrier is very close to the 42.9 kcal/mol predicted by Lewis and co-workers[11] calculated at the B3LYP/6-311g(d,p) level of theory. The barrier calculated by Chakraborty et al.[10] is slightly higher (44.6 kcal/mol) at the B3LYP/6-31g(d) level of theory. This is due to the smaller basis set used. From INT9, we examined two pathways: HONO and MN eliminations.

INT9 eliminates an MN from the eight-membered ring to form INT10 through the transition state TS12. INT10 is a six-membered ring, with the same structure as RDX after eliminating the first HONO molecule. The barrier height of this step is 33.9 kcal/mol, which is much lower than the barrier height of 41.0 kcal/mol for eliminating the second HONO from HMX reported by Chakraborty et al.[10] INT10 eliminates another MN to form a chain-structure INT11 by passing the transition state TS13 that has the barrier of 38.5 kcal/mol. INT11 then eliminates an HONO to form the intermediate INT12 via the transition state TS14 with a barrier height of 35.9 kcal/mol. INT12 decomposes into CN and H_2CN, with a very high barrier of 103.9 kcal/mol passing over the transition state TS15. This indicates that INT12 is quite stable and difficult for unimolecular decomposition. The species with the same molar mass as INT12 (54) has been detected in mass spectroscopy. It is possible that INT12 further decomposes via a bimolecular reaction channel.

The second decomposition pathway is the elimination of another HONO from INT9 to form INT13 through the transition state TS16. The calculated barrier height for this step is 41.7 kcal/mol, which is close to the value of 41.0 kcal/mol obtained by Chakraborty et al.[10] INT13 eliminates an MN from the eight-membered ring to form INT14 with a low barrier of 20.5 kcal/mol via the transition state TS17. INT14 forms INT15 by

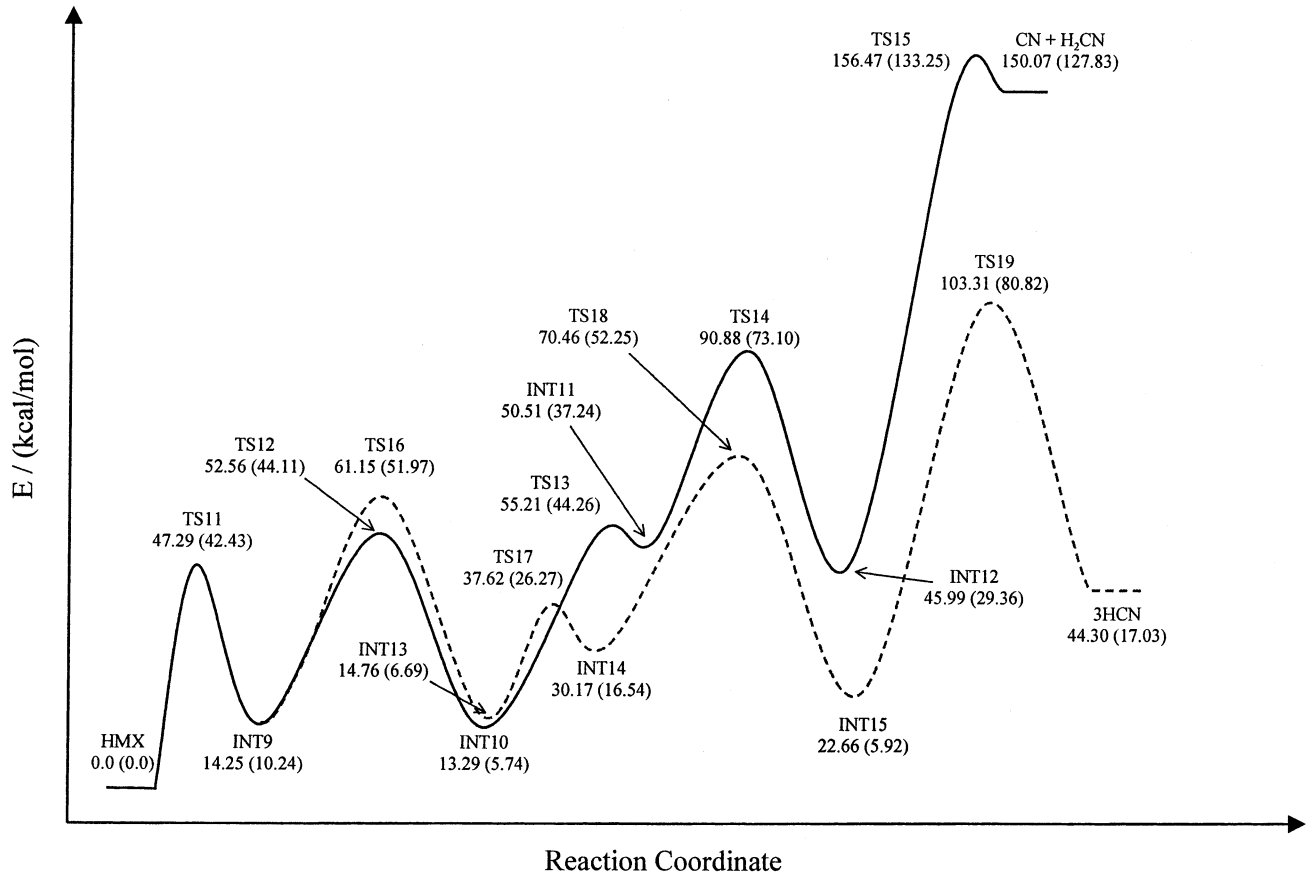

Figure 4. Relative energies of the HONO elimination pathway. The data in parentheses are zero-point-energy corrected relative energies. See Figure 3 for notations of species.

TABLE 1: Arrhenius Parameters for the Elementary Reactions of the HMX Decomposition[a]

reactions	A	n	E_a/R
NNO_2 Fission Path			
HMX → HMR[b]	2.15×10^{17}	−0.52	19 124
HMR → INT1	1.95×10^{13}	0.25	10 985
INT1 → INT2	7.96×10^{10}	0.14	9 138
INT2 → INT3	2.63×10^{13}	0.41	11 573
INT3 → INT4	3.22×10^{12}	0.36	5 468
INT4 → INT5	9.67×10^{12}	0.32	10 285
INT5 → INT6	6.50×10^{11}	−0.06	2 259
INT6 → H_2CN+ H_2CO	4.21×10^{13}	0.09	3 605
INT1 → INT7	5.86×10^{12}	0.28	11 132
INT7 → INT8	1.31×10^{13}	0.27	11 190
INT8 → H_2CN + MN	4.80×10^{12}	0.24	5 654
HONO Elimination Path			
HMX → INT9[b,c]	9.67×10^{12}	0.11	19 913
INT9 → INT10	6.46×10^{13}	0.54	18 099
INT10 → INT11	7.16×10^{12}	0.46	20 035
INT11 → INT12[c]	3.59×10^{8}	1.45	16 918
INT12 → CN + H_2CN	1.07×10^{12}	0.84	52 884
INT9 → INT13[c]	2.96×10^{6}	2.04	19 159
INT13 → INT14	2.15×10^{14}	0.36	10 700
INT14 → INT15[c]	1.78×10^{9}	1.31	17 067
INT15 → 3HCN[c]	1.60×10^{11}	0.92	37 952

[a] The Arrhenius expression is in the form of $k(T) = A\,T^n\,e^{(-\,Ea/RT)}$. The parameters are calculated by fitting the TST rate constants to this expression. [b] Rate constants are calculated using the muVT method from ref. [c] Quantum transmission effects were calculated using the Eckart method for these reactions involving hydrogen migration.

eliminating another HONO through the transition state TS18 with a barrier height of 35.7 kcal/mol. Finally, INT15 decomposes into three HCN through a hydrogen shift with a high barrier height of 74.9 kcal/mol via the transition state TS19.

TABLE 2: Calculated Heat of Formations at 298 K of the Intermediates Involved in the Decomposition Pathways

species	$\Delta H_f°(298)$ (kcal/mol)	reactions for calculating $\Delta H_f°(298)$
HMX	23.60	$4H_2 + 4N_2 + 4CO_2 = HMX$
HMR	63.43	$4H_2 + 3N_2 + 3CO_2 + CN = HMR$
INT1	73.38	$4H_2 + 3N_2 + 3CO_2 + CN = INT1$
INT2	77.51	$4H_2 + 3N_2 + 3CO_2 + CN = INT2$
INT3	97.62	$4H_2 + 3N_2 + 3CO_2 + CN = INT3$
INT4	82.22	$3H_2 + 2N_2 + 2CO_2 + H_2CO + CN = INT4$
INT5	72.39	$2H_2 + N_2 + CO_2 + H_2CO + CN = INT5$
INT6	23.14	$H_2CO + H_2 + CN = INT6$
INT7	70.04	$3H_2 + 2N_2 + 2CO_2 + CN = INT7$
INT8	64.11	$2H_2 + N_2 + CO_2 + CN = INT8$
INT9	57.19	$3H_2 + 3N_2 + 3CO_2 + HCN = INT9$
INT10	32.23	$2H_2 + 2N_2 + 2CO_2 + HCN = INT10$
INT11	43.65	$H_2 + N_2 + CO_2 + HCN = INT11$
INT12	59.35	$2HCN = INT12$
INT13	77.17	$2H_2 + 2N_2 + 2CO_2 + 2HCN = INT13$
INT14	67.35	$H_2 + N_2 + CO_2 + 2HCN = INT14$
INT15	80.37	$3HCN = INT15$
MN	21.38	$H_2 + N_2 + CO_2 = MN$
H_2CN	49.52	$H_2 + CN = H_2CN$
H_2CO	−27.70[a]	
CN	104.0[a]	
CO_2	−94.05[a]	
HCN	32.30[a]	
NO_2	7.91[a]	
NNO	19.61[a]	
HONO	−18.34[a]	

[a] Experimental results from NIST database.[37] Notice that $\Delta H_f°(298)$ of H_2 and N_2 are 0.0 by definition.

The highest barriers of the two decomposition pathways following the first HONO elimination are 103.9 and 74.9 kcal/mol, which are lower than the highest barrier of 106.7 kcal/

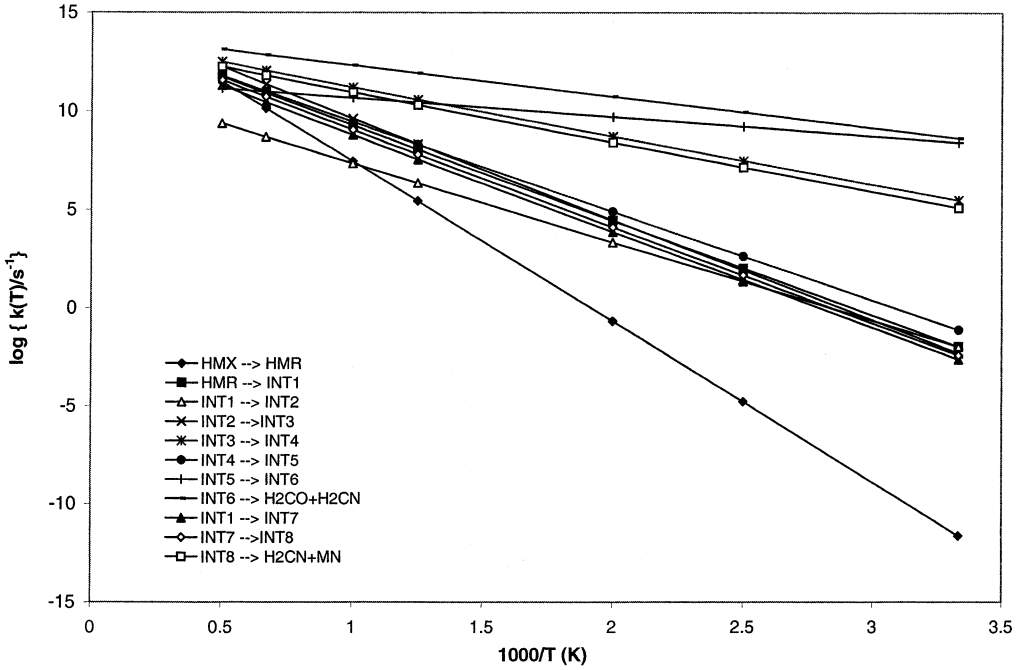

Figure 5. Arrehenius plots of the rate constants of the elementary reactions of the N−NO_2 fission pathway.

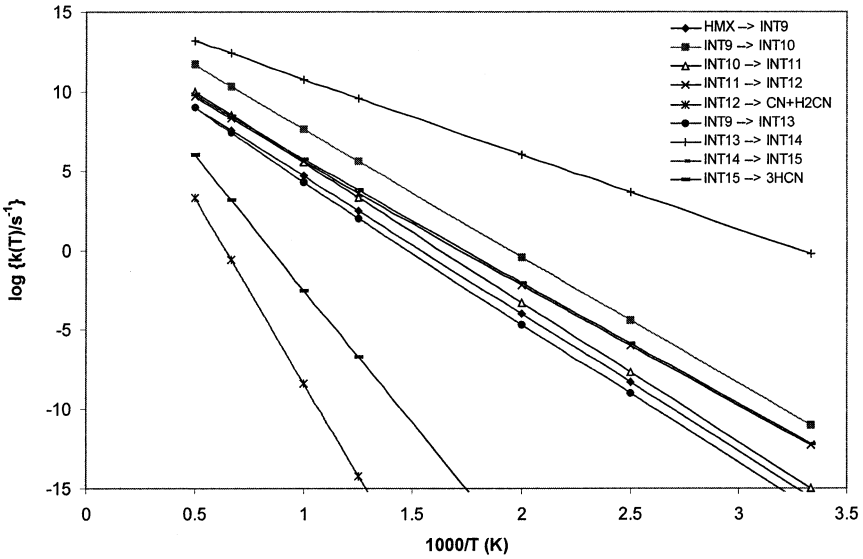

Figure 6. Arrhenius plots of the rate constants of the elementary reactions of the HONO elimination fission pathway. Tunneling effects are included in the rate constants of HONO elimination reactions using the Eckart method.

mol of the 4-HONO successive decomposition reactions proposed earlier.[10] In particular, the highest energy transition state, TS18 relative to HMX (80.8 kcal/mol), of the second pathway is also lower than that of 87.4 kcal/mol of the 4-HONO successive decomposition reactions.[10]

3.2. Comparisons of Calculated Intermediates with Mass Spectroscopy Observations. Since numerous mass spectroscopy and pyrolysis experiments have been carried out for HMX, it is a reasonable to verify the mechanism by comparing the measured species with the calculated intermediates despite the fact that most experimental data were measured in the condensed phase.

In mass spectroscopy experiments, all the intermediates have been identified as major products for the three MN successive elimination channel after HMR breaks the second-nearest-neighbor C−N bond in the N−NO_2 fission pathway (HMX → HMR(m=250) → INT1(m=250) → INT7(m=176) → INT8(m=102)). However, for the other channel of the N−NO_2 fission pathway, namely, HMX → HMR(m=250) → INT1(m=250) → INT2(m=250) → INT3(m=250) → INT4(m=206) → INT5(m=132) → INT6(m=58), the masses of the last three intermediates were not identified. This may be due to the differences in the mechanisms for the gas phase and condensed phase since the ring closure from INT1 to INT2 may be difficult in the condensed phase. Another possibility is that the rate from INT1 to INT2 is much slower than that from INT1 to INT7. This is in fact the case, as discussed below. For the HONO elimination pathway, all the intermediates were identified except for INT11(m=101) and INT13(m=202). INT13 is a key species for successive decompositions. The lack of INT13 shows that the species of mass m = 128 and m = 81 may be produced by other mechanisms. Notice that the species involved in the HONO elimination pathway are minor observed products as compared with those in the N−NO_2 fission pathway.

In the pyrolysis of HMX, all the intermediates have been observed for the N−NO_2 fission pathways. However, the masses

TABLE 3: Calculated Thermodynamics Parameters in the CHEMKIN Format As Defined in Equations 2−4[a]

	HMX		HMR		INT1		INT2	
	300−1500 K	1500−5000 K	300−1500 K	1500−5000 K	300−1500 K	1500−5000 K	300−1500 K	1500−5000 K
a1	−5.200 643 36	$2.592\,968\,81 \times 10^{-2}$	−5.712 073 98	$2.251\,161\,89 \times 10^{-2}$	−2.151 618 41	$2.271\,311\,89 \times 10^{-2}$	−5.734 687 07	$2.264\,481\,76 \times 10^{-2}$
a2	$1.633\,575\,31 \times 10^{-1}$	$9.115\,253\,98 \times 10^{-2}$	$1.461\,176\,61 \times 10^{-1}$	$8.056\,055\,74 \times 10^{-2}$	$1.373\,421\,36 \times 10^{-1}$	$8.069\,647\,72 \times 10^{-2}$	$1.479\,715\,38 \times 10^{-1}$	$8.066\,684\,29 \times 10^{-2}$
a3	$-1.459\,373\,85 \times 10^{-4}$	$-3.931\,326\,14 \times 10^{-5}$	$-1.301\,852\,19 \times 10^{-4}$	$-3.460\,388\,52 \times 10^{-5}$	$-1.212\,802\,91 \times 10^{-4}$	$-3.470\,223\,10 \times 10^{-5}$	$-1.336\,911\,85 \times 10^{-4}$	$-3.467\,814\,75 \times 10^{-5}$
a4	$6.562\,059\,24 \times 10^{-8}$	$7.492\,201\,70 \times 10^{-9}$	$5.861\,146\,54 \times 10^{-8}$	$6.578\,261\,08 \times 10^{-9}$	$5.438\,136\,20 \times 10^{-8}$	$6.602\,216\,50 \times 10^{-9}$	$6.096\,525\,37 \times 10^{-8}$	$6.595\,954\,53 \times 10^{-9}$
a5	$-1.179\,261\,14 \times 10^{-11}$	$-5.261\,143\,69 \times 10^{-13}$	$-1.056\,480\,82 \times 10^{-11}$	$-4.611\,782\,99 \times 10^{-13}$	$-9.789\,482\,01 \times 10^{-12}$	$-4.631\,201\,23 \times 10^{-13}$	$-1.110\,760\,20 \times 10^{-11}$	$-4.625\,912\,62 \times 10^{-13}$
a6	$7.329\,496\,18 \times 10^{3}$	$8.148\,018\,86 \times 10^{3}$	$2.816\,801\,49 \times 10^{4}$	$2.862\,566\,15 \times 10^{4}$	$3.243\,394\,00 \times 10^{4}$	$3.362\,849\,40 \times 10^{4}$	$3.520\,414\,02 \times 10^{4}$	$3.570\,672\,21 \times 10^{4}$
a7	$5.691\,969\,70 \times 10$	$5.840\,799\,86 \times 10$	$5.705\,730\,76 \times 10$	$5.186\,627\,54 \times 10$	$4.387\,229\,50 \times 10$	$5.767\,975\,90 \times 10$	$5.654\,749\,66 \times 10$	$5.189\,475\,42 \times 10$

	INT3		INT4		INT5		INT6	
	300−1500 K	1500−5000 K	300−1500 K	1500−5000 K	300−1500 K	1500−5000 K	300−1500 K	1500−5000 K
a1	−2.142 285 62	$2.310\,851\,70 \times 10^{-2}$	$-7.077\,890\,81 \times 10$	$1.981\,985\,86 \times 10^{-2}$	$2.397\,748\,73 \times 10^{-1}$	$1.321\,534\,69 \times 10^{-2}$	$-1.307\,982\,28 \times 10^{-1}$	$5.856\,389\,51 \times 10^{-3}$
a2	$1.391\,799\,27 \times 10^{-1}$	$8.114\,583\,62 \times 10^{-2}$	$1.195\,457\,41 \times 10^{-1}$	$7.053\,505\,85 \times 10^{-2}$	$7.876\,051\,17 \times 10^{-2}$	$4.725\,875\,19 \times 10^{-2}$	$3.453\,148\,09 \times 10^{-2}$	$2.330\,644\,76 \times 10^{-2}$
a3	$-1.239\,425\,51 \times 10^{-4}$	$-3.499\,908\,55 \times 10^{-5}$	$-1.084\,342\,46 \times 10^{-4}$	$-3.029\,373\,81 \times 10^{-5}$	$-7.207\,183\,94 \times 10^{-5}$	$-2.026\,787\,02 \times 10^{-5}$	$-2.683\,711\,07 \times 10^{-5}$	$-9.776\,921\,21 \times 10^{-6}$
a4	$5.585\,784\,91 \times 10^{-8}$	$6.670\,414\,78 \times 10^{-9}$	$5.013\,917\,42 \times 10^{-8}$	$5.760\,044\,95 \times 10^{-9}$	$3.378\,535\,63 \times 10^{-8}$	$3.850\,581\,09 \times 10^{-9}$	$1.105\,420\,14 \times 10^{-8}$	$1.831\,296\,27 \times 10^{-9}$
a5	$-1.008\,714\,02 \times 10^{-11}$	$-4.684\,336\,50 \times 10^{-13}$	$-9.285\,381\,97 \times 10^{-12}$	$-4.039\,250\,25 \times 10^{-13}$	$-6.344\,654\,28 \times 10^{-12}$	$-2.698\,863\,97 \times 10^{-13}$	$-1.893\,659\,22 \times 10^{-12}$	$-1.271\,236\,80 \times 10^{-13}$
a6	$4.456\,576\,17 \times 10^{4}$	$4.580\,643\,86 \times 10^{4}$	$3.713\,555\,05 \times 10^{4}$	$3.849\,012\,98 \times 10^{4}$	$3.342\,870\,78 \times 10^{4}$	$3.449\,501\,67 \times 10^{4}$	$1.036\,383\,23 \times 10^{4}$	$1.068\,867\,35 \times 10^{4}$
a7	$4.640\,468\,55 \times 10$	$6.091\,732\,03 \times 10$	$3.441\,336\,92 \times 10$	$5.355\,351\,21 \times 10$	$2.916\,838\,68 \times 10$	$4.589\,768\,46 \times 10$	$2.625\,652\,95 \times 10$	$3.109\,002\,86 \times 10$

	INT7		INT8		INT9		INT10	
	300−1500 K	1500−5000 K	300−1500 K	1500−5000 K	300−1500 K	1500−5000 K	300−1500 K	1500−5000 K
a1	$-9.670\,951\,86 \times 10^{-1}$	$1.605\,106\,69 \times 10^{-2}$	$8.461\,742\,57 \times 10^{-2}$	$9.310\,187\,58 \times 10^{-3}$	−4.571 040 16	$2.200\,339\,39 \times 10^{-2}$	3.371 116 38	$1.519\,771\,98 \times 10^{-2}$
a2	$9.532\,864\,08 \times 10^{-2}$	$5.735\,513\,74 \times 10^{-2}$	$5.352\,470\,88 \times 10^{-2}$	$3.391\,994\,00 \times 10^{-2}$	$1.391\,908\,13 \times 10^{-1}$	$7.767\,992\,63 \times 10^{-2}$	$9.628\,218\,64 \times 10^{-2}$	$5.417\,152\,14 \times 10^{-2}$
a3	$-8.316\,963\,92 \times 10^{-5}$	$-2.463\,288\,21 \times 10^{-5}$	$-4.536\,352\,91 \times 10^{-5}$	$-1.450\,246\,74 \times 10^{-5}$	$-1.241\,094\,56 \times 10^{-4}$	$-3.347\,006\,94 \times 10^{-5}$	$-8.454\,073\,23 \times 10^{-5}$	$-2.329\,113\,09 \times 10^{-5}$
a4	$3.699\,179\,09 \times 10^{-8}$	$4.682\,696\,07 \times 10^{-9}$	$1.981\,001\,23 \times 10^{-8}$	$2.749\,286\,21 \times 10^{-9}$	$5.577\,242\,03 \times 10^{-8}$	$6.374\,776\,02 \times 10^{-9}$	$3.746\,724\,13 \times 10^{-8}$	$4.430\,197\,27 \times 10^{-9}$
a5	$-6.625\,554\,94 \times 10^{-12}$	$-3.282\,955\,48 \times 10^{-13}$	$-3.510\,925\,96 \times 10^{-12}$	$-1.923\,955\,99 \times 10^{-13}$	$-1.002\,442\,94 \times 10^{-11}$	$-4.474\,675\,75 \times 10^{-13}$	$-6.654\,664\,31 \times 10^{-12}$	$-3.106\,967\,93 \times 10^{-13}$
a6	$3.196\,291\,15 \times 10^{4}$	$3.290\,129\,90 \times 10^{4}$	$3.021\,952\,19 \times 10^{4}$	$3.087\,283\,94 \times 10^{4}$	$2.494\,467\,07 \times 10^{4}$	$2.560\,152\,84 \times 10^{4}$	$1.362\,270\,44 \times 10^{4}$	$1.400\,592\,01 \times 10^{4}$
a7	$3.724\,722\,27 \times 10$	$4.967\,744\,77 \times 10$	$2.873\,717\,87 \times 10$	$3.904\,817\,03 \times 10$	$5.173\,279\,39 \times 10$	$5.207\,835\,84 \times 10$	$4.603\,881\,59 \times 10$	$4.480\,116\,12 \times 10$

	INT11		INT12		INT13		INT14	
	300−1500 K	1500−5000 K	300−1500 K	1500−5000 K	300−1500 K	1500−5000 K	300−1500 K	1500−5000 K
a1	$7.016\,942\,39 \times 10^{-1}$	$8.707\,075\,39 \times 10^{-3}$	2.108 411 33	$4.559\,305\,87 \times 10^{-3}$	−3.930 969 64	$1.805\,607\,18 \times 10^{-2}$	$5.303\,558\,73 \times 10^{-1}$	$1.143\,170\,35 \times 10^{-2}$
a2	$4.777\,306\,83 \times 10^{-2}$	$3.093\,388\,70 \times 10^{-2}$	$2.043\,850\,27 \times 10^{-2}$	$1.721\,904\,90 \times 10^{-2}$	$1.154\,499\,89 \times 10^{-1}$	$6.416\,169\,99 \times 10^{-2}$	$6.379\,239\,59 \times 10^{-2}$	$4.081\,266\,76 \times 10^{-2}$
a3	$-4.053\,892\,68 \times 10^{-5}$	$-1.329\,942\,51 \times 10^{-5}$	$-1.502\,268\,62 \times 10^{-5}$	$-7.295\,413\,13 \times 10^{-6}$	$-1.033\,039\,74 \times 10^{-4}$	$-2.759\,904\,70 \times 10^{-5}$	$-5.406\,825\,10 \times 10^{-5}$	$-1.753\,004\,09 \times 10^{-5}$
a4	$1.760\,158\,94 \times 10^{-8}$	$2.529\,986\,30 \times 10^{-9}$	$5.931\,396\,68 \times 10^{-9}$	$1.375\,508\,40 \times 10^{-9}$	$4.668\,371\,39 \times 10^{-8}$	$5.251\,325\,95 \times 10^{-9}$	$2.344\,580\,16 \times 10^{-8}$	$3.332\,771\,20 \times 10^{-9}$
a5	$-3.091\,333\,26 \times 10^{-12}$	$-1.774\,594\,37 \times 10^{-13}$	$-9.893\,316\,83 \times 10^{-13}$	$-9.592\,117\,9 \times 10^{-14}$	$-8.440\,892\,70 \times 10^{-12}$	$-3.683\,721\,64 \times 10^{-13}$	$-4.113\,194\,39 \times 10^{-12}$	$-2.336\,732\,77 \times 10^{-13}$
a6	$1.995\,987\ 66 \times 10^{4}$	$2.070\,269\,00 \times 10^{4}$	$2.845\,268\,00 \times 10^{4}$	$2.916\,335\,01 \times 10^{4}$	$3.569\,714\,68 \times 10^{4}$	$3.620\,856\,99 \times 10^{4}$	$3.133\,355\,23 \times 10^{4}$	$3.222\,475\,07 \times 10^{4}$
a7	$2.570\,843\,40 \times 10$	$3.873\,242\,66 \times 10$	$1.554\,956\,15 \times 10$	$3.110\,395\,81 \times 10$	$4.695\,697\,44 \times 10$	$4.638\,878\,30 \times 10$	$2.913\,918\,30 \times 10$	$4.411\,249\,00 \times 10$

	INT15		MN	
	300−1500 K	1500−5000 K	300−1500 K	1500−5000 K
a1	1.669 404 14	$7.267\,913\,68 \times 10^{-3}$	$9.794\,244\,70 \times 10^{-1}$	$6.000\,159\,02 \times 10^{-3}$
a2	$3.728\,356\,38 \times 10^{-2}$	$2.707\,834\,42 \times 10^{-2}$	$3.186\,243\,43 \times 10^{-2}$	$2.106\,572\,54 \times 10^{-2}$
a3	$-2.959\,147\,18 \times 10^{-5}$	$-1.151\,305\,96 \times 10^{-5}$	$-2.752\,362\,55 \times 10^{-5}$	$-9.077\,008\,74 \times 10^{-6}$
a4	$1.236\,284\,33 \times 10^{-8}$	$2.175\,286\,59 \times 10^{-9}$	$1.218\,987\,30 \times 10^{-8}$	$1.729\,291\,53 \times 10^{-9}$
a5	$-2.134\,515\,43 \times 10^{-12}$	$-1.518\,984\,60 \times 10^{-13}$	$-2.181\,085\,08 \times 10^{-12}$	$-1.214\,212\,28 \times 10^{-13}$
a6	$3.852\,809\,34 \times 10^{4}$	$3.933\,672\,50 \times 10^{4}$	$9.271\,410\,14 \times 10^{3}$	$9.898\,242\,18 \times 10^{3}$
a7	$1.991\,129\,81 \times 10$	$3.604\,882\,81 \times 10$	$2.218\,309\,34 \times 10$	$3.395\,686\,52 \times 10$

[a] Parameters a1−a5 were calculated by fitting the pressure heat capacities to eq 2. Then, a6 was calculated by substituting a1−a5 and heat of formation at 298 K into eq 3. Parameter a7 was obtained by averaging the results that were calculated by substituting a1−a5 and standard entropies at different temperatures in to eq 4.

of $m = 202$ and $m = 101$ of the HONO elimination pathway are still not detected. This suggests that the $N-NO_2$ fission pathways are the dominant channels in the decomposition of HMX. In particular, the HMX → HMR → INT1 → INT7 → INT8 → H_2CN + MN is perhaps the most important channel.

3.3. Thermal Rate Constants. We have calculated the rate constants using the TST theory for all elementary steps of the pathways discussed in the previous section. The rate constants of the initiate steps of both pathways were taken from our previous muVT calculation.[13,14] The last step (INT6 → H_2CO + H_2CN) of the $N-NO_2$ fission pathway does not have a transition state; thus its rate constants were not calculated here. However, one would expect this reaction to be very fast and would therefore not have a large influence on the overall rate. For those reactions that involve HONO elimination, tunneling effects were also calculated using the Eckart method.[36] The calculated thermal rate constants were further fitted to the Arrhenius expression in the form of $k(T) = A\ T^n\ e^{(-Ea/RT)}$.

Table 1 lists the Arrhenius parameters of the elementary reactions. Figures 5 and 6 show the plots of rate constants versus temperature for both $N-NO_2$ fission and HONO elimination pathways, respectively. It can be seen that in the $N-NO_2$ fission path, the initial step, the HMX → HMR reaction, has the lowest rate constants at temperatures below 1000 K. Thus, this reaction is the rate-controlling step of the overall path at low temperatures, i.e., below 1000 K. However, the reaction INT1 → INT2 becomes the slowest for temperatures above 1000 K. Since this reaction is the first step of the ring-closure pathway, the other mechanism, MN elimination, dominates the $N-NO_2$ fission pathway in this temperature range. This conclusion is in agreement with the product distribution of Behrens' measurements. In fact, the INT1 → INT2 reaction is the slowest reaction after the first $N-NO_2$ fission step at temperatures above 400 K. Accordingly, the MN elimination mechanism virtually dominates this pathway in the whole temperature range where one can observe sufficient HMX decomposition. In the HONO elimination pathway, the rate-controlling reactions are the last steps of the two mechanisms due to their high barrier heights. In particular, most of the reactions in the HONO elimination pathway are slower than the reactions in the $N-NO_2$ fission path in the whole temperature range as depicted in Figures 5 and 6. Thus, the $N-NO_2$ fission pathways dominate the gas-phase decomposition of HMX.

3.4. Thermodynamics Parameters. We calculated the thermodynamic properties of all the stable species using statistical thermodynamics theory based on the translational, rotational, and vibrational information from quantum chemistry calculations. The constant pressure heat capacities were first employed to fit eq 2 to obtain the CHEMKIN format parameters a1−a5. Then, parameter a6 was calculated by substituting a1−a5 and heat of formation at 298 K of the corresponding species into eq 3. Parameter a7 was determined by averaging the results that were calculated by substituting a1−a5 and standard entropies at different temperatures into eq 4. The evaluated heats of formation at 298 K of all the species are listed in Table 2. The calculated CHEMKIN format parameters a1−a7 for each species are summarized in Table 3.

4. Conclusion

We have presented in this work a detailed density functional theory study of the thermal decomposition mechanism of the gas-phase α-HMX. Thermal rate constants of all elementary reactions, as well as thermodynamic parameters of all intermediate species, were calculated by TST theory and statistical thermodynamics methods, respectively. We found four new low-lying energy channels among which two channels belong to the $N-NO_2$ fission pathway and the two others belonging to the HONO elimination pathway. The final products of these channels are in agreement with the most abundant products observed experimentally. From analysis of the rate constants, the dominant pathway is as follows: HMX loses a NO_2 molecule at the initial step and then breaks the second-nearest-neighbor C−N bond to have a chain structure. The chain structure successively loses three methylenenitramine molecules. The final products of this channel are 1 mol of NO_2 and of H_2CN and 3 mol of methylenenitramine for each mole of decomposed HMX. The methylenenitramine can further decompose into H_2CO and NNO easily under catalysis of water and/or other molecules. This product distribution is the same as those observed experimentally by Behrens.[24]

Acknowledgment. This work is supported by the University of Utah Center for the Simulation of Accidental Fires & Explosions, funded by the Department of Energy, Lawrence Livermore National Laboratory, under Subcontract B341493, and a generous gift from the Dow Chemical Co. The authors would like to thank the Utah Center for High Performance Computing for computer time support.

References and Notes

(1) Yetter, R. A.; Dryer, F. L.; Allen, M. T.; Gatto, J. L. *J. Propul. Power* **1995**, *11*, 683.
(2) Melius, C. F. Thermochemical Modeling: I. Application to Decomposition of Energetic Materials. In *Chemistry and Physics of Energetics Materials*; Bulusu, S. N., Ed.; Kluwer Academic: Dordrecht, The Netherlands, 1990.
(3) Chakraborty, D.; Muller, R. P.; Dasgupta, S.; Goddard, W. A., III. *J. Phys. Chem. A* **2000**, *104*, 2261.
(4) Harris, N. J.; Lammertsma, K. *J. Am. Chem. Soc.* **1997**, *119*, 6583.
(5) Johnson, M. A.; Truong, N. T. *J. Phys. Chem. A* **1999**, *103*, 8840.
(6) Manaa, M. R.; Fried, L. E. *J. Phys. Chem. A* **1999**, *102*, 9884.
(7) Pai, S. V.; Chabalowski, C. F.; Rice, B. M. *J. Phys. Chem.* **1996**, *100*, 15368.
(8) Rice, B. M.; Chabalowski, C. F. *J. Phys. Chem. A* **1997**, *101*, 8720.
(9) Wu, C. J.; Fried, L. E. *J. Phys. Chem. A* **1997**, *101*, 8675.
(10) Chakraborty, D.; Muller, R. P.; Dasgupta, S.; Goddard, W. A., III. *J. Phys. Chem. A* **2001**, *105*, 1302.
(11) Lewis, J. P.; Glaesemann, K. R.; VanOpdorp, K.; Voth, G. A. *J. Phys. Chem. A* **2000**, *104*, 11384.
(12) Melius, C. F. *J. Phys. Colloq.* **1987**, *48*, 341.
(13) Zhang, S.; Truong, N. T. *J. Phys. Chem. A* **2000**, *104*, 7304.
(14) Zhang, S.; Truong, N. T. *J. Phys. Chem. A* **2001**, *105*, 2427.
(15) Suryanarayana, B.; Graybush, R. J.; Autera, J. R. *Chem. Ind.* **1967**, *52*, 2177.
(16) Bulusu, S.; Axenrod, T.; Miline, G. W. A. *Org. Mass. Spectrom.* **1970**, *3*, 13.
(17) Farber, M.; Srivastava, R. D. Proceedings of the 16th JANNAF Combustion Meeting. *CPIA Publ.* **1979**, *308*, 59.
(18) Morgan, C. V.; Bayer, R. A. *Combust. Flame* **1979**, *36*, 99.
(19) Schroeder, M. Proceedings of the 16th JANNAF Combustion Meeting. *CPIA Publ.* **1979**, *308*, 17.
(20) Fifer, R. A. In *Fundamentals of Solid Propellant Combustion, Progress in Astronautics*; Kuo, K. K., Summerfield, M., Eds.; AIAA Inc.: New York, 1984; Vol. 90, p 177.
(21) Tang, C.-J.; Lee, Y. J.; Kudva, G.; Litzinger, T. A. *Combust. Flame* **1999**, *117*, 170.
(22) Tang, C.-J.; Lee, Y. J.; Litzinger, T. A. *J. Propul. Power* **1999**, *15*, 296.
(23) Brill, T. B. *J. Propul. Power* **1995**, *11*, 740.
(24) Behrens, R., Jr. *J. Phys. Chem.* **1990**, *94*, 6706.
(25) Truhlar, D. G.; Garrett, B. C.; Klippenstein, S. J. *J. Phys. Chem.* **1996**, *100*, 12771.
(26) Zhang, S.; Truong, N. T. VKLab, http://vklab.hec.utah.edu, 2001.
(27) McQuarrie, D. A. *Statistical thermodynamics*; Harper & Row: New York, 1973.
(28) Kee, R. J.; Miller, J. A.; Jefferson, T. H. *Proceedings of the Summer Computer Simulation Conference*; Society for Computer Simulation International: San Diego, CA, 1981.
(29) Becke, A. D. *J. Chem. Phys.* **1993**, *98*, 5648.

(30) Woon, D. E.; Dunning, T. H., Jr. *J. Chem. Phys.* **1993**, *98*, 1358.
(31) Frisch, M. J.; Trucks, G. W.; Schlegel, H. B.; Scuseria, G. E.; Robb, M. A.; Cheeseman, J. R.; Zakrzewski, V. G.; Montgomery, J. A., Jr.; Stratmann, R. E.; Burant, J. C.; Dapprich, S.; Millam, J. M.; Daniels, A. D.; Kudin, K. N.; Strain, M. C.; Farkas, O.; Tomasi, J.; Barone, V.; Cossi, M.; Cammi, R.; Mennucci, B.; Pomelli, C.; Adamo, C.; Clifford, S.; Ochterski, J.; Petersson, G. A.; Ayala, P. Y.; Cui, Q.; Morokuma, K.; Malick, D. K.; Rabuck, A. D.; Raghavachari, K.; Foresman, J. B.; Cioslowski, J.; Ortiz, J. V.; Stefanov, B. B.; Liu, G.; Liashenko, A.; Piskorz, P.; Komaromi, I.; Gomperts, R.; Martin, R. L.; Fox, D. J.; Keith, T.; Al-Laham, M. A.; Peng, C. Y.; Nanayakkara, A.; Gonzalez, C.; Challacombe, M.; Gill, P. M. W.; Johnson, B. G.; Chen, W.; Wong, M. W.; Andres, J. L.; Head-Gordon, M.; Replogle, E. S.; Pople, J. A. *Gaussian 98*, revision A.7; Gaussian, Inc.: Pittsburgh, PA, 1998.
(32) Chio, C. S.; Boutin, H. P. *Acta Crystallogr. B* **1970**, *26*, 1235.
(33) Cady, H. H.; Larson, A. C.; Cromer, D. T. *Acta Crystallogr.* **1963**, *16*, 617.
(34) Cobbledick, R. E.; Small, R. W. H. *Acta Crystallogr.* **1974**, *30*, 1918.
(35) Behrens, R., Jr. *J. Phys. Chem.* **1991**, *95*, 5838.
(36) Miller, W. H. *J. Am. Chem. Soc.* **1979**, *101*, 6810.
(37) Chase, M. W. J. *J. Phys. Chem. Ref. Data, Monogr.* **1998**, *9*, 1.